UNIVERSITÀ DEGLI STUDI DI PADOVA

Dipartimento di Fisica e Astronomia "Galileo Galilei"

Corso di Laurea in Astronomia

Tesi di Laurea

Validation of equilibrium initial conditions for stellar systems through N-body simulations

Validazione delle condizioni iniziali all'equilibrio per sistemi stellari attraverso simulazioni N-corpi

Relatore

Christos Efthymiopoulos

Laureando

Giulia Manconi

Anno Accademico 2022/2023

Abstract

The aim of this thesis is to develop a numerical method to produce equilibrium initial conditions for a galactic system. In the first phase the different components of the galaxy (halo, bulge and disc) are considered separately. Subsequently, the interaction between them is taken into account in the final method to produce the initial conditions of the N-Body particles. Eddington' formula is used to get the distribution function of the bodies for the components with spherical symmetry. For the disc, instead, Toomre's law and Jeans equations are considered. The numerical method builds a logarithmic grid with the parameters of density, potential, dispersion and velocities of the bodies. This grid is used to generate the initial conditions, that are then validated as regards the maintenance of the collisionless equilibrium using a parallel-mesh code for gravitational N-body systems.

Italian section

Abstract

L'obiettivo di questa tesi è quello di sviluppare un metodo numerico per la produzione di condizioni iniziali dei corpi di una galassia in equilibrio. Prima si considerano separatamente le sue componenti (alone, bulge e disco). Successivamente si considera l'interazione tra di esse per generare le condizioni iniziali. Per le componenti a simmetria sferica si sfrutta la formula di Eddinghton per calcolare la funzione di distribuzione, mentre per il disco si considerano la legge di Toumre e le equazioni di Jeans per ottenere le condizioni iniziali. Il metodo numerico usato si basa sulla produzione di una griglia logaritmica in cui vengono inseriti tutti i parametri di densità, potenziale, dispersione e velocità dei corpi. La griglia viene sfruttata per la generazione delle condizioni iniziali del sistema che vengono poi validate tramite l'uso di un codice parallel- mesh per sistemi gravitazionali di N-corpi.

Riassunto

Per la generazione delle condizioni iniziali delle componenti a simmetria sferica si sfrutta la formula di Eddington al fine di definire la funzione di distribuzione dei corpi. In primo luogo si costruisce una griglia in cui, a raggi equidistanti, si calcolano il valore del potenziale e della densità. Per poter usare la formula di Eddington (1), e quindi ottenere la funzione di distribuzione, si costruisce un'altra griglia che a valori equidistanti del potenziale associa raggio e densità corrispondenti, calcolati tramite interpolazione. Ora si può calcolare l'integrale della formula di Eddington e ottenere f.

$$f_{(\epsilon)} = \frac{1}{\sqrt{8}\pi^2}\frac{\mathrm{d}}{\mathrm{d}\epsilon}\int_{\epsilon}^{V_{(r_{max})}} \frac{\mathrm{d}\rho_{(\mathrm{r})}}{\mathrm{dV}_{(\mathrm{r})}}\frac{dV_{(r)}}{\sqrt{V_{(r)}-\epsilon}} \tag{1}$$

A questo punto si possono ottenere le condizioni iniziali: si considerano una serie di valori equidistanti per raggi e velocità e per ogni coppia di essi si determina il valore di (2) costruendo una griglia tridimensionale.

$$F_{(\vec{r},\vec{v})} = f_{(\epsilon_{(\vec{r},\vec{v})})} 16\pi^2 r^2 v^2 \tag{2}$$

Scegliendo una distribuzione uniforme di raggio, velocità e F compresi tra zero e il loro valore massimo ottenuto precedentemente, si vanno a considerare solo le coppie (r, v) tali che il valore di F associato ad esse sia inferiore rispetto a quello che si ha nella griglia tridimensionale. Si ripete questa procedura fino ad ottenere N=10^6 corpi di cui si avranno le coordinate sferiche. Per poter verificare la stabilità del sistema bisogna però passare alle coordinate cartesiane sfruttando una distribuzione uniforme per gli angoli che si formano con i piani xy e xz.

Questa procedura si applica sia per l'alone, in cui a partire dalla formula (3) si ottiene il potenziale usando (4), che per il bulge, in cui per la densità si considera una legge di Sérsic.

$$\rho(r) = \frac{M_{halo}}{2\pi}\frac{a}{r}\frac{1}{(a+r)^3} \tag{3}$$

$$V(r) = -\frac{G}{r}\int_0^r 4\pi r'^2\rho(r')\mathrm{d}r' - G\int_r^{\infty} 4\pi r'\rho(r')\mathrm{d}r' \tag{4}$$

Per la generazione delle condizioni iniziali del disco galattico non si può sfruttare questo procedimento, in quanto viene a mancare la simmetria sferica del sistema. La tecnica utilizzata in questo caso è quella di costruire una griglia a partire da valori equidistanti del raggio a cui associare la misura della densità superficiale e del potenziale con cui si determinano frequenza epiciclica e angolare. Sfruttando le equazioni di Jeans si ottiene il valore medio della velocità angolare in funzione del raggio. Con la legge di Toumre si ottengono i valori della dispersione in direzione radiale e angolare. A questo punto si considera una nuova griglia, in cui vengono considerati raggi in scala logaritmica, e si determinano tutti i valori precedentemente calcolati tramite interpolazione quantificando il numero di corpi in ogni cella. In questo modo si hanno le informazioni necessarie per ottenere le condizioni iniziali dei corpi del disco generando distribuzioni uniformi dei corpi attorno al raggio considerato e distribuzioni gaussiane di velocità la cui dispersione è nota ad ogni raggio.

Una volta considerate le componenti in maniera separata si sfruttano delle tecniche di rilassamento per avere un sistema stabile quando esse vengono unite. A questo scopo si utilizza un codice che permette lo studio dell'evoluzione temporale del sistema a partire dalle condizioni iniziali prodotte. In primo luogo si rilassa l'alone, congelando i corpi del disco e facendo evolvere il sistema finché non appare in equilibrio; successivamente si congela l'alone lasciando evolvere il disco.

A questo punto con il nuovo disco e il nuovo alone entrambi stabilizzati si ottiene una galassia stabile.

.

Contents

Chapter 1

Theoretical introduction

To simulate a galactic system using the N-body method we need to find a way to describe the initial distribution of the bodies' positions and velocities. In the present thesis we discuss how to obtain initial conditions for N-body simulations of a galaxy with three components: halo, bulge and disc. In chapter 2 and 3 is explained how to calculate the initial conditions of the spheroidal components and of the disc respectively (following a procedure similar the one used in Kyziropoulos et al. [2016]). Section 4 describes the method employed to relax all the components of the galaxy when they are put all together and interact. Section 5 explains how our method to produce initial conditions is validated, by examining how the galaxy evolves after relaxation and up to what extent, the equilibrium state is mantained in time.

1.1 The distribution function and its moments

A fundamental quantity for the description of stellar systems is the distribution function(DF) $f(\vec{r}, \vec{v}, t)$, which defines the numerical density of bodies in the phase-space at time t:

$$f(\vec{r}, \vec{v}, t) = \frac{\Delta N}{\Delta^3 \vec{r} \Delta^3 \vec{v}} \tag{1.1}$$

This function can also be interpreted as the probability of finding a body with given phase-space coordinates at time t. Assuming all bodies identical the DF is normalised such that:

$$\int d^3\vec{r} d^3\vec{v} f(\vec{r}, \vec{v}, t) = 1 \tag{1.2}$$

Integrating the distribution function over velocities yields the bodies' numerical density per unit volume (1.3).

$$\rho(t, \vec{r}) = \int f(\vec{r}, \vec{v}, t) \mathrm{d}^3\tilde{\mathrm{v}} \tag{1.3}$$

The dispersion of velocities in x-axis direction is given by

$$\begin{gathered} \sigma_x^2(\vec{r}, t) = \frac{1}{\rho(\vec{r}, t)} \int (v_x(\vec{r}, t) - \overline{v_x(\vec{r}, t)})^2 f(\vec{r}, \vec{v}, t) \mathrm{d}^3\tilde{\mathrm{v}} \\ \text{where } \overline{v_x(\vec{r}, t)} = \int v_x(\vec{r}, t) f(\vec{r}, \vec{v}, t) \mathrm{d}^3\tilde{\mathrm{v}} \end{gathered} \tag{1.4}$$

and similarly are defined the velocity dispersions σ_y and σ_z. In order to describe the orbit of the bodies we consider the Hamiltonian:

$$H(\vec{p}, \vec{q}, t) = \frac{\vec{p}^2}{2} + V(\vec{r}, t) \tag{1.5}$$

where the potential can be obtained solving Poisson's equation:

$$\nabla^2 V = 4\pi G\rho \tag{1.6}$$

By the well known Liouville's theorem for the Hamiltonians systems we have

$$\begin{gathered}\frac{\mathrm{df}(\mathbf{p},\mathbf{q})}{\mathrm{dt}}=0\\ \frac{\partial f}{\partial t}+\dot{\mathbf{q}}\frac{\partial f}{\partial \mathbf{q}}-\nabla V\frac{\partial f}{\partial \mathbf{p}}=0\end{gathered} \tag{1.7}$$

Equation (1.7) is known as collisionless Boltzmann equation.

A stellar system is said to be in steady state equilibrium if:

$$\frac{\partial f}{\partial t}=0 \tag{1.8}$$

In the case of steady state equilibrium, equation (1.7) can be written as

$$\vec{v}\frac{\partial f}{\partial \vec{r}}-\frac{\partial V}{\partial \vec{r}}\frac{\partial f}{\partial \vec{v}}=0 \tag{1.9}$$

A useful set of equations can be obtained by calculating the momenta of the distribution function with respect to the velocities.
The zero momentum is obtained by:

$$\int_{-\infty}^{+\infty}\mathrm{d^3v}\left(\vec{v}\frac{\partial f}{\partial \vec{r}}-\frac{\partial V}{\partial \vec{r}}\frac{\partial f}{\partial \vec{v}}\right)=0 \tag{1.10}$$

Splitting the integral into its summed terms we final:

$$\begin{gathered}\int_{-\infty}^{+\infty}\mathrm{d^3v}\left(v_x\frac{\partial f}{\partial x}+v_y\frac{\partial f}{\partial y}+v_z\frac{\partial f}{\partial z}\right)=\frac{\partial}{\partial x}(\rho_{(\vec{r},t)}\overline{v_x})+\frac{\partial}{\partial y}(\rho_{(\vec{r},t)}\overline{v_y})+\frac{\partial}{\partial z}(\rho_{(\vec{r},t)}\overline{v_z})\\ \int_{-\infty}^{+\infty}\mathrm{d^3v}\left(\frac{\partial V}{\partial \vec{r}}\frac{\partial f}{\partial \vec{v}}\right)=\frac{\partial V}{\partial x}\int_{-\infty}^{+\infty}\mathrm{dv_x dv_y dv_z}\frac{\partial f}{\partial v_x}+\frac{\partial V}{\partial y}\int_{\infty}^{+\infty}\mathrm{d^3v}\frac{\partial f}{\partial v_y}+\frac{\partial V}{\partial z}\int_{\infty}^{+\infty}\mathrm{d^3v}\frac{\partial f}{\partial v_z}=\\ =\frac{\partial V}{\partial x}\left(f|_{-\infty}^{+\infty}-\int_{-\infty}^{+\infty}\mathrm{d^3v}f\right)+\frac{\partial V}{\partial y}\int_{-\infty}^{+\infty}v_x\mathrm{dv_x dv_z}[f_{v_y=+\infty}-f_{v_y=-\infty}]+\frac{\partial V}{\partial z}\int_{-\infty}^{+\infty}v_x\mathrm{dv_x dv_y}[f_{v_z=+\infty}-f_{v_z=-\infty}]\\ =0\end{gathered}$$

as well as

$$\int_{-\infty}^{+\infty}\mathrm{d^3v}v_x f_{(\vec{r},\vec{v},t)}=\int v_x\frac{\Delta N}{\Delta x\Delta y\Delta z\Delta v_x\Delta v_y\Delta v_z}\Delta v_x\Delta v_y\Delta v_z=\rho\overline{v_x} \tag{1.11}$$

Hence the zero-order Jeans equation takes the form:

$$\frac{\partial}{\partial x}(\rho\overline{v_x})+\frac{\partial}{\partial y}(\rho\overline{v_y})+\frac{\partial}{\partial z}(\rho\overline{v_z})=0 \tag{1.12}$$

Which represents the continuity equation in the usual space of the bodies' motions.

The first momentum of Jeans equation yields:

$$\int_{-\infty}^{\infty}\mathrm{d^3v}v_x\left(\vec{v}\frac{\partial f}{\partial \vec{r}}-\frac{\partial V}{\partial \vec{r}}\frac{\partial f}{\partial \vec{v}}\right)=0 \tag{1.13}$$

(1.13) can be solved splitting it into the two addends and given that the distribution function is 0 when $v=\infty$:

$$\begin{gathered}\int_{-\infty}^{+\infty}\mathrm{d^3v}\left(v_x^2\frac{\partial f}{\partial x}+v_xv_y\frac{\partial f}{\partial y}+v_xv_z\frac{\partial f}{\partial z}\right)=\frac{\partial}{\partial x}(\rho_{(\vec{r},t)}\overline{v_x^2})+\frac{\partial}{\partial y}(\rho_{(\vec{r},t)}\overline{v_xv_y})+\frac{\partial}{\partial z}(\rho_{(\vec{r},t)}\overline{v_xv_z})\\ \int_{-\infty}^{+\infty}\mathrm{d^3v}v_x\left(\frac{\partial V}{\partial \vec{r}}\frac{\partial f}{\partial \vec{v}}\right)=\frac{\partial V}{\partial x}\int_{-\infty}^{+\infty}\mathrm{dv_x dv_y dv_z}v_x\frac{\partial f}{\partial v_x}+\frac{\partial V}{\partial y}\int_{\infty}^{+\infty}\mathrm{d^3v}v_x\frac{\partial f}{\partial v_y}+\frac{\partial V}{\partial z}\int_{\infty}^{+\infty}\mathrm{d^3v}v_x\frac{\partial f}{\partial v_z}=\\ =\frac{\partial V}{\partial x}\left(v_xf|_{-\infty}^{+\infty}-\int_{-\infty}^{+\infty}\mathrm{d^3v}f\right)+\frac{\partial V}{\partial y}\int_{-\infty}^{+\infty}v_x\mathrm{dv_x dv_z}[f_{v_y=+\infty}-f_{v_y=-\infty}]+\frac{\partial V}{\partial z}\int_{-\infty}^{+\infty}v_x\mathrm{dv_x dv_y}[f_{v_z=+\infty}-f_{v_z=-\infty}]\\ =-\frac{\partial V}{\partial x}\rho_{(\vec{r},t)}\end{gathered} \tag{1.14}$$

Hence:

$$\begin{aligned}
\frac{\partial}{\partial x}(\rho\overline{v_x^2}) + \frac{\partial}{\partial y}(\rho\overline{v_x v_y}) + \frac{\partial}{\partial z}(\rho\overline{v_x v_z}) + \frac{\partial V}{\partial x}\rho = 0 \\
\frac{\partial}{\partial y}(\rho\overline{v_y^2}) + \frac{\partial}{\partial x}(\rho\overline{v_x v_y}) + \frac{\partial}{\partial z}(\rho\overline{v_y v_z}) + \frac{\partial V}{\partial y}\rho = 0 \\
\frac{\partial}{\partial z}(\rho\overline{v_z^2}) + \frac{\partial}{\partial x}(\rho\overline{v_x v_z}) + \frac{\partial}{\partial y}(\rho\overline{v_y v_z}) + \frac{\partial V}{\partial z}\rho = 0
\end{aligned} \tag{1.15}$$

1.2 Stellar equilibrium for spherical systems

According to Jeans theorem, in a spherical system the distribution function depends on the coordinates (r, v) through the integrals of motion (ϵ, L) where:

$$\epsilon(r, \vec{v}) = \frac{v_x^2 + v_y^2 + v_z^2}{2} + V(r) \tag{1.16}$$

is the energy and

$$L = \vec{r} \wedge \vec{v} \tag{1.17}$$

is the angular momentum.

Consider the case in which the dispersion of velocities at each point of space satisfies the condition $\sigma_x^2 = \sigma_y^2 = \sigma_z^2$. In such case the system is called isotropic.
In the case of an isotropic system the distribution function depends on ϵ. Switching to spherical coordinates $(v_x, v_y, v_z) \to (v, \theta, \phi)$ from equation (1.3) we final

$$\begin{gathered}
\mathrm{dv_x dv_y dv_z} = v^2 \sin\theta \mathrm{dv d\theta d\phi} \\
\rho(r) = \int f(r, \vec{v})\mathrm{d\tilde{v}^3} = \int_0^\pi \mathrm{d}\theta \sin\theta \int_0^{2\pi} \mathrm{d}\phi \int_0^\infty v^2 \mathrm{dv} f(\tfrac{v^2}{2} + V(r)) = 4\pi \int_0^\infty v^2 \mathrm{dv} f(\tfrac{v^2}{2} + V(r)) = \\
= 4\pi \int_{V(r)}^{V_{min}} \sqrt{2(\epsilon - V(r))} f(\epsilon) \mathrm{d}\epsilon \\
\frac{\rho(r)}{\sqrt{8}\pi} = 2\int_{V(r)}^{V_{min}} \sqrt{\epsilon - V(r)} f(\epsilon) \mathrm{d}\epsilon
\end{gathered} \tag{1.18}$$

Differentiating both sides of (1.18) we obtain

$$\frac{d\rho(r)}{\sqrt{8}\pi dV} = \int_{V(r)}^{V_{min}} \frac{f(\epsilon)}{\sqrt{\epsilon - V(r)}} \mathrm{d}\epsilon \tag{1.19}$$

The Abel integral (1.19)can be inverted leading to Eddington's formula(this procedure is described in chapter 4 Binney and Tremaine [1987]).

$$f(\epsilon) = \frac{1}{\sqrt{8}\pi^2} \frac{\mathrm{d}}{\mathrm{d}\epsilon} \int_\epsilon^{V_{(r_{max})}} \frac{\mathrm{d}\rho(\mathrm{r})}{\mathrm{dV(r)}} \frac{dV(r)}{\sqrt{V(r) - \epsilon}} \tag{1.20}$$

This integral is easily solved if the equations for ρ and V are known.

The density $\rho(r)$ is obtained by observations of the brighteness profile of the galaxy.

The potential of a galaxy is calculated using Poisson equation (1.6) whose solution is

$$V(r) = -\frac{G}{r}\int_0^r 4\pi r'^2 \rho(r')\mathrm{dr}' - G\int_r^\infty 4\pi r' \rho(r')\mathrm{dr}' \tag{1.21}$$

At this point f is expressed in the terms of energy ϵ and radius r and hence in terms of (r, v).

Consider now a spherical shell of radius r and volume $4\pi r^2 dr$, as well as a shell in velocity space of volume $4\pi v^2 dv$. The number of particles within the shell is given by:

$$\Delta N = f(r, v) 16\pi^2 r^2 v^2 \Delta r \Delta v \tag{1.22}$$

Using spherical coordinates we can distribute the ΔN particles uniformly within the shell volumes, by setting uniform distributions in the angular parameters:

$$\begin{gathered} -1 \leq \cos(\theta) \leq 1 \\ 0 \leq \phi \leq 2\pi \\ -1 \leq \cos(\theta_v) \leq 1 \\ 0 \leq \phi_v \leq 2\pi \end{gathered} \tag{1.23}$$

We then assign cartesian positions and velocities to the particles via the formulas:

$$\begin{gathered} x = r\sin\theta\cos\phi \\ y = r\sin\theta\sin\phi \\ z = r\cos\theta \\ v_x = v\sin\theta_v\cos\phi_v \\ v_y = v\sin\theta_v\sin\phi_v \\ v_z = v\cos\theta_v \end{gathered} \tag{1.24}$$

1.3 Equilibria of stellar discs

We use cylindrical coordinates to describe a flat disc of zero thickness. The collisioless Boltzmann equation(1.7) takes the form

$$\frac{\partial f}{\partial t} + p_R\frac{\partial f}{\partial r} + \frac{p_\phi}{r^2}\frac{\partial f}{\partial \phi} - \left(\frac{\partial V}{\partial r} - \frac{p_\phi^2}{r^3}\right)\frac{\partial f}{\partial p_R} - \frac{\partial V}{\partial \phi}\frac{\partial f}{\partial p_\phi} = 0 \tag{1.25}$$

Setting $\frac{\partial f}{\partial t} = 0$ we obtain Jeans' equations for a disc in steady-state equilibrium. Multiplying (1.25) by p_R and integrating over the momenta and considering that $\rho = \Sigma(r)r$ where $\Sigma(r)$ is the surface density we arrive at:

$$\frac{\partial(\Sigma\overline{v_R^2})}{\partial r} + \Sigma\frac{\partial V}{\partial r} + \frac{\Sigma}{r}(\overline{v_R^2} - \overline{v_\phi^2}) = 0 \tag{1.26}$$

We consider the case where $\overline{v_R} = 0$, $\overline{v_\phi} = \mu_\phi$, $\overline{v_R^2} = \sigma_R^2$, $\overline{v_\phi^2} = \mu_\phi^2 + \sigma_\phi^2$, and adopt an exponential profile $\Sigma(r) = \Sigma_0 e^{-r/R_D}$
The dispersion of velocities can be obtained using Toomre's Q parameter:

$$Q(r) = \frac{\sigma_R(r)\kappa(r)}{3.36G\Sigma(r)} \tag{1.27}$$

where κ and Ω are angular and epicyclic frequencies.

$$\Omega(r) = \sqrt{\frac{1}{r}\frac{\partial V}{\partial r}} \tag{1.28}$$

$$\kappa(r) = \sqrt{\frac{3}{r}\frac{\partial V}{\partial r} + \frac{\partial^2 V}{\partial r^2}} \tag{1.29}$$

We adopt an exponential law for Toomre's parameter, leading to the asymptotic values $Q = Q_0$ for $r = 0$ and $Q = Q_\infty$ for $r = \infty$.

Once the profile Q(r) has been selected, we can compute the radial and azimuthal dispertions profiles via the formulas

$$\sigma_R(r) = \frac{3.36G\Sigma(r)Q(r)}{\kappa(r)} \tag{1.30}$$

$$\sigma_\phi(r) = \frac{\kappa(r)\sigma_R(r)}{2\Omega(r)} \tag{1.31}$$

Once the dispersion of velocities is known, we can compute $\mu_\phi(r)$ via the Jeans equation(1.26) leading to the asymmetric drift formula.

$$\mu_\phi(r) = \sqrt{\frac{r}{\Sigma(r)}\frac{\partial(\Sigma(r)\sigma_R^2(r))}{\partial r} + r\frac{\partial V(r)}{\partial r} + \sigma_R^2(r) - \sigma_\phi^2(r)} \tag{1.32}$$

Finally we locally approximate the distribution of velocities within a ring of radius R by the Gaussian formula:

$$f_R(v_R, v_\phi) = \frac{1}{2\pi\sigma_R\sigma_\phi} e^{-\frac{v_R^2}{2\sigma_R^2} - \frac{(v_\phi - \mu_\phi)^2}{2\sigma_\phi^2}} \tag{1.33}$$

Chapter 2

Initial conditions for spheroidal components

We consider a spherical galctic component where we aim to get the initial conditions of the bodies in cartesian coordinates. There are two distinct spherical components in our model of galaxy: bulge and halo. We find the initial conditions of the bodies in each of them using a similar procedure, starting from different density laws.

2.1 Halo

For the halo we consider a spherical model with a density profile law (the same used in Hernquist [1990])

$$\rho(r) = \frac{M_{halo}}{2\pi}\frac{a}{r}\frac{1}{(a+r)^3} \tag{2.1}$$

Where a is the scale radius and M_{halo} is the total mass of the halo. We set $a = 5kpc$ and $M_{halo} = 2 \cdot 10^{10} M\odot$ and build a linear grid calculating the density at each $r_i = i\Delta r$ where $\Delta r = 0.01$ and $i = 1, ..., 3000$ corresponding to $R_{max} = 30kpc$ and $R_{min} = 0.01kpc$. This model for the density profile should result in a Hernquist model for the potential.

$$V(r) = -\frac{GM_{halo}}{r+a} \tag{2.2}$$

Figure 2.1 shows the potential obtained using the Hernquist profile via equation (1.21). We use the trapezoidal method to calculate the integrals. This method calculates the area subtended by a function adding the areas of the trapezoids that have as vortex two points of infinitesimal ranges of the domain and their corresponding values of the function. It is clear from the image that the values somewhat differ. This is due to the truncation of the galaxy inside the radius R_{max}. By the comparison the potential can be fixed just subtracting from the analytic potential the difference between the analytic and the Hernquist potential at R_{max}. In this way the two profiles now coincide as in figure 2.2.

Now we have a linear grid with parameters r_i, ρ_i and $V(r_i)$ and we aim to get the distribution function using Eddington formula (1.20). A convenient way to calculate this integral, considering that it uses infinitesimal potential, is to build another grid where we have equidistant potentials and their correspondent values of radius and density. Therefore we consider $V(R_{max})$ and $V(R_{min})$ to build the new grid, where $V_j = j\Delta V$ where $\Delta V = \frac{V(R_{max})-V(R_{min})}{1000-1}$ and $j = 0, ..., 1000$. To get the values of radius and density correspondent to the j-potentials, we can use the linear interpolation formula

$$\begin{aligned} r_j &= r_i + \tfrac{r_{i+1}-r_i}{V_{i+1}-V_i}(V_j - V_i) \\ \rho_j &= r_i + \tfrac{\rho_{i+1}-\rho_i}{V_{i+1}-V_i}(V_j - V_i) \end{aligned} \tag{2.3}$$

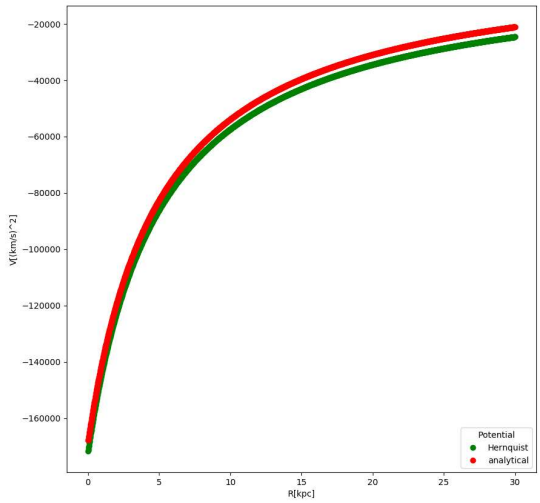

Figure 2.1: Comparison between Hernquist profile and values of potential obtained with 1.21

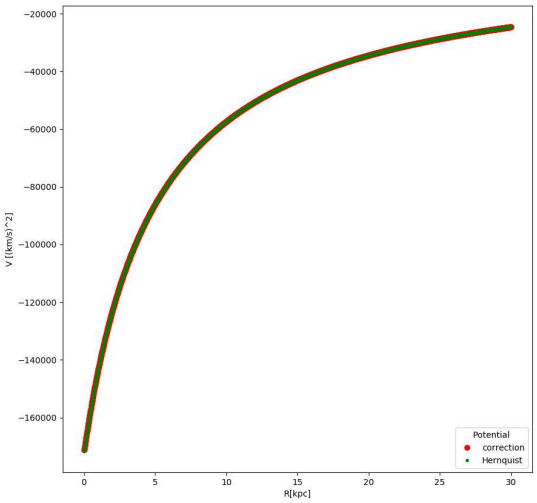

Figure 2.2: Potential corrected after comparison with Hernquist profile

where i and $i+1$ are the indexes of the linear grid in which we find V_j . Once we have this grid, we can calculate the distribution function using equation (1.20) where we replicate for ϵ the V_j values. The theoretical distribution function for the hernquist model is (2.4)(as we can see in Hernquist [1990])

$$f(V) = \frac{M_{tot}}{8\sqrt{2}\pi^3 a^3 v_g^3} \frac{1}{(1-q^2)^{\frac{5}{2}}} (3\arcsin q + q + q(1-q^2)^{\frac{1}{2}}(1-2q^2)(8q^4 - 8q^2 - 3)$$
$$v_g = \left(\frac{GM_{tot}}{a}\right)^{\frac{1}{2}} \tag{2.4}$$
$$q = \sqrt{-\frac{a}{GM_{tot}}V}$$

As shown in figure (2.6), the distribution function we obtained is a good approximation, it is different

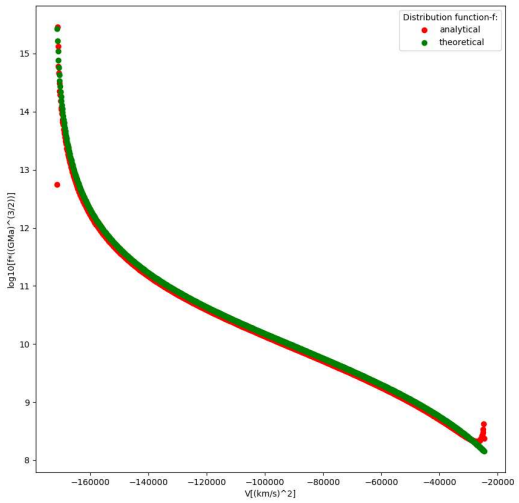

Figure 2.3: Comparison between theoric and analytic distribution function

from the theoretical one only at very small or large values of energy. For large E the difference is caused by the fact that we're considering all the bodies as they were inside radius R_{max}. At small energy the error is due to the use of a finite grid.

Now we consider the function (1.22) and we calculate a grid with $N_k = 1000$ values of $F = \frac{\Delta N}{\Delta r \Delta v}$ just to have an approximatiom for its maximum value. Therefore we consider the N_k values $r_k = k\Delta r$ ($\Delta r = \frac{R_{max}}{k-1}$) and $v_{k'} = k'\Delta v$ ($\Delta v = \frac{v_{max}}{k'-1}$ where $v_{max} = \sqrt{2V_{i=0}}$ and $k, k' = 1, ...N_k$); for each possible couple $(r_k, v_{k'})$ we calculate F at each couple of radius and velocity.

To build this 3-dimentional grid, we start from the radia r_k and calculate the correspondent potential using the linear interpolation formula 2.3 starting from V_j and r_j. For each r_k we calculate the possible energy per mass with $v_{k'}$, using 2.5.

$$E_{kk'} = \frac{1}{2}v_{k'}^2 + V_k \tag{2.5}$$

We can now calculate $f_{kk'}$ with 2.3 starting from f_j, V_j and using the energy $E_{kk'}$. We have now r_k, $v_{k'}$ and $f_{kk'}$ to calculate the 3-dimentional grid of the $F(\vec{r_k}, \vec{v_{k'}})$ values(calculated using equation (1.22)). We are ready to get the initial conditions.

We produce values of r, v, F distributed uniformly in the ranges: $0 < r < R_{max}$, $0 < v < v_{max}$ and $0 < F < F_{max}$. We consider $N_{halo} = 10^6$ triplettes (r, v, F), where $F < F(r, v))$ with $F(r, v)$ obtained by the quadratic interpolation using the values of the 3-dimensional grid (2.6).

$$\begin{gathered}
r_1 = \Delta r \lfloor (\tfrac{r}{\Delta r}) \rfloor \\
r_2 = \Delta (1 + r \lfloor (\tfrac{r}{\Delta r}) \rfloor) \\
v_1 = \Delta v \lfloor (\tfrac{v}{\Delta v}) \rfloor \\
v_2 = \Delta (1 + v \lfloor (\tfrac{v}{\Delta v}) \rfloor) \\
F_{00} = F(r_1, v_1) \\
F_{10} = \tfrac{F(r_2, v_1) - F(r_1, v_1)}{\sigma r} \\
F_{01} = \tfrac{F(r_1, v_2) - F(r_1, v_1)}{\sigma v} \\
F(r, v) = F_{00} + F_{10}(r - r_1) + F_{01}(v - v_1)
\end{gathered} \tag{2.6}$$

Choosing the (r, v) of the triplettes, where we have $F(r, v) < F$ we obtained the initial spherical conditions. The best way to manipulate the data is using cartesian coordinates, therefore we use (1.24) to transform the coordinates.

Once we have this set of initial conditions for the halo, the centre of gravity of the galaxy needs to correspond to the origin of the axes. Therefore we use equation (2.7) for the coordinates x, y, z to correct the position of bodies.

$$\begin{gathered}
x_{cg} = \frac{\sum_{i=1}^{N_{tot}} x_i \cdot m_i}{\sum_{i=1}^{N_{tot}} m_i} \\
x_{new} = x_i - x_{vg}
\end{gathered} \tag{2.7}$$

Also the velocities are corrected according to

$$\begin{gathered}
v_{cg} = \frac{\sum_{i=1}^{N_{tot}} v_i \cdot m_i}{\sum_{i=1}^{N_{tot}} m_i} \\
v_{new} = v_i - v_{vg}
\end{gathered} \tag{2.8}$$

2.2 Bulge

For the bulge we consider a Sérsic density profile

$$\begin{gathered}
\rho_{B(r)} = -\tfrac{1}{\pi} \int_r^\infty \tfrac{\mathrm{d}\Sigma_{\mathrm{B(R)}}}{\mathrm{dR}} \tfrac{1}{\sqrt{R^2 - r^2}} \mathrm{dR} \\
\Sigma_{B(r)} = \Sigma_0 e^{-b_B (r/r_B)^{\frac{1}{n_B}} - 1}
\end{gathered} \tag{2.9}$$

where Σ_0 is the central surface density given by

$$\Sigma_0 = \frac{M_{bulge}}{\int_0^\infty 2\pi s e^{-b_B(s/r_B)^{\frac{1}{n_B}}-1}\mathrm{ds}} \tag{2.10}$$

where

$$\int_0^\infty 2\pi s e^{-b_B(s/r_B)^{\frac{1}{n_B}}-1}\mathrm{ds} = 2\pi r_B^2 \tag{2.11}$$

To obtain initial conditions for the bulge bodies we follow the same procedure used for the halo. The Sérsic profile considered has the following parameters: $M_{bulge} = 5 \cdot 10^9 M\odot$, $n_B = 3.5$, $r_B = 1.5kpc$, $b_B = 2n_B - 0.324$. In 2.4 we can see the potential profile, it is clear that it is really high inside the

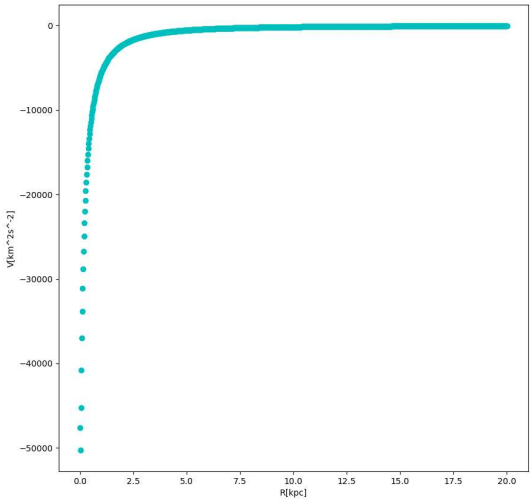

Figure 2.4: Potential in the bulge

scale radius r_B, then it decreases rapidly because all the mass of the bulge is concentrated in the inner part of the galaxy. Then we switch to the grid with equidistant potentials and determine the distribution function shown in figure (2.5). The bodies are concentrated in the centre of the galaxy,

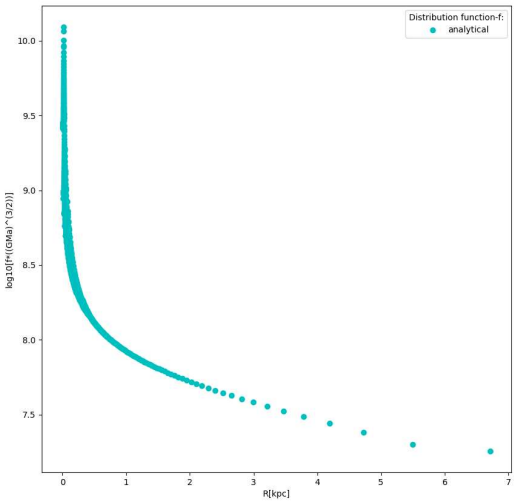

Figure 2.5: Bulge distribution function

according to the fact that we are considering the bulge. Once we have the distribution function we obtain the initial conditions in the same way as the halo, using equations (2.5) and (2.6).

2.3 Test

Once we have the initial conditions, we study their distribution and see if the results are compatible with what expected.

The spheres of the halo and the bulge are divided in concentric shells $\Delta r = \frac{R_{max}}{N_{shell}}$ wide (we considered $N_{shell} = 100$). Knowing the radius of each body, we can count how many bodies there are in each shell(ΔN) and get the numerical distribution(2.12).

$$\rho(\vec{r}) = \frac{\Delta N}{4\pi r^2 \Delta r} \tag{2.12}$$

2.3.1 Halo

Comparing 2.12 with 2.1 we can check how accurate is the method we used to get the initial conditions. It seems clear that the bodies are distributed correctly up to the radius of about 5 kpc, then we see

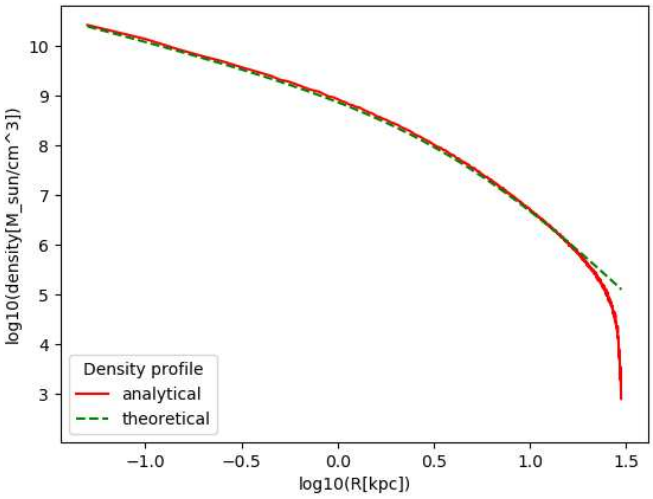

Figure 2.6: Density test with a logarithmic scale for the halo

that the calculated density decreases much faster than the model. This happens because we chose a=5kpc as scale radius for the density profile, therefore at this radius the density is cut off.

2.3.2 Bulge

Comparing (2.9) with (2.12), we can see how accurate are the bulge initial conditions. Figure (2.7) shows that the density of bodies in the bulge is higher than density in the halo if we consider the inner part of the galaxy. Analysing the plot it results that the profile is close to the theoretical profile inside radius of $r \approx 3.5kpc$, in the outer region it has a different trend, this is probably due to the fact that when we build the grid with equidistant potential $V(R_{max})$ and $V(R_{min})$ are far apart and consequently many bodies are counted in the last cell of the grid, thus increasing the density at large radii.

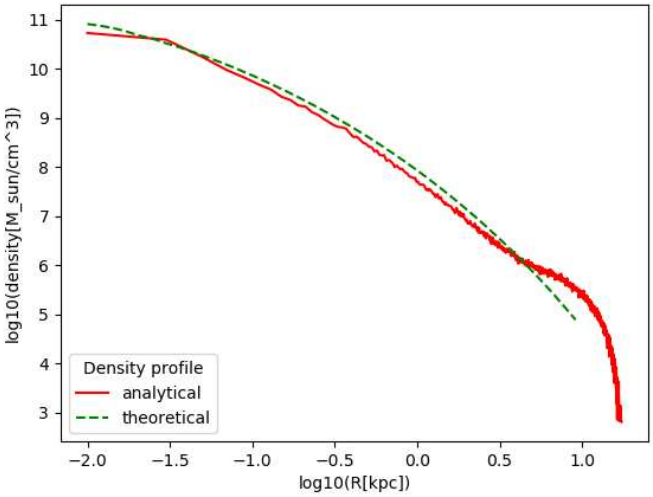

Figure 2.7: Density test with logarithmic scale for the bulge

Chapter 3

Initial conditions for disc components

The first step to get the initial conditions for the bodies in the disc is to calculate the potential at a given radius. The maximum and minimum disc radii considered are $R_{max} = 20kpc$ and $R_{min} = 0.1kpc$ and total mass of the disc is $M_{disc} = 5 \cdot 10^9 M\odot$. We create a linear grid starting from the values of radii $r_i = i\Delta r$ where $\Delta r = R_{max}/N_L$, $i = 1, ..., N_L$ and $N_L = 200$.

The disc's surface density law is exponential (3.2) and $\Sigma_0 = 1.8 \cdot 10^9 \odot /kpc^2$ value is calculated solving equation (3.1).

$$M_{disc} = \int_0^\infty \Sigma_0 e^{\frac{-R_D}{r}} 2\pi r \mathrm{d}r \tag{3.1}$$

$$\Sigma(r_i) = \Sigma_0 e^{-r_i/R_D} \tag{3.2}$$

where $R_D = 3kpc$. The density law is corrected at the edges of the grid in order to decrease the number of bodies and make the disc more similar to reality. The functions for the correction are 3.3.

$$\begin{aligned} f_1(r) &= \tfrac{1}{2} + \tfrac{1}{2}\tanh\left(\tfrac{r-3R_{min}}{R_{min}}\right) \\ f_2(r) &= \tfrac{1}{2} + \tfrac{1}{2}\tanh\left(-\tfrac{r-0.9R_{max}}{10R_{min}}\right) \end{aligned} \tag{3.3}$$

Multiplying this function by $\Sigma(R)$ we obtain the density profile shown in figure 3.1. The system is

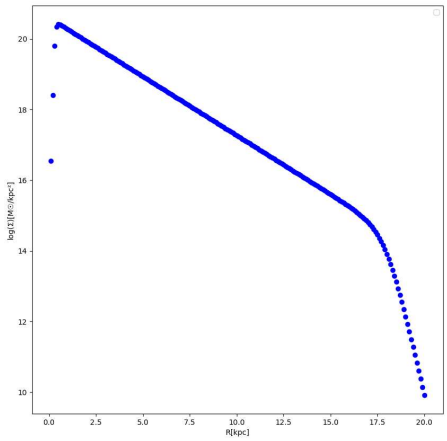

Figure 3.1: Density profile of the disc

not perfectly flat, to reproduce the thickness of the disc we can consider the bodies as they were distributed randomly inside the area defined by the exponential function (3.4):

$$f(z) = e^{-z/z_D} \tag{3.4}$$

The mean velocity $\overline{v_z} = 0$ and the dispersion of velocities follows:

$$\sigma_z(r) = \sigma_R(r) e^{z_D/R_D} \tag{3.5}$$

The potential can now be estimated via the formula

$$\begin{gathered} V(r_i) = -\int \frac{G\mathrm{dm}}{\|\vec{r_i} - \vec{R'}\|} = -\int_0^\infty \mathrm{dR'} \int_0^{2\pi} \mathrm{d}\phi \frac{GR'\Sigma(R')}{(r_i^2 + R'^2 + 2r_i R' \cos\phi)^{\frac{1}{2}}} \\ \mathrm{dm} = \Sigma(R')\mathrm{d}\sigma = \Sigma(R')R'\mathrm{dR'}\mathrm{d}\phi \end{gathered} \tag{3.6}$$

Considering the fact that we need to run a simulation of the disc and the halo we add to the potential

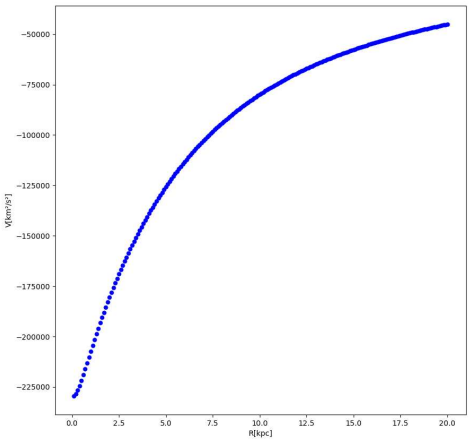

Figure 3.2: Disco potential

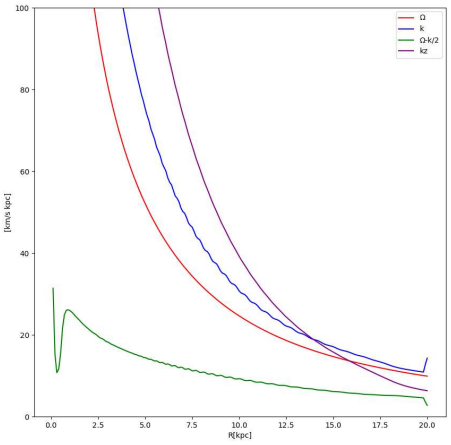

Figure 3.3: k and omega

of the disc the potential of the halo calculated in (2.1). The value of the potential obtained is shown in figure 3.2 in which we can see that the potential increases its absolute value getting closer to the galactic centre.

Once we know the potential, we can determine the values of the angular and epicyclic frequencies $\Omega(r_i)$ and $\kappa(r_i)$ (1.28, 1.29).

The result for angular and epicyclic frequencies is shown in figure 3.3 where the blue curve is κ and the red curve is Ω. In the plot is shown the value of $\Omega - \kappa/2$ with a green line: such value should be constant for most of the extension of the disc; as we see in the graph, this condition is fulfilled. These two frequences are needed to calculate the dispersion of velocities(1.30,1.31, 3.5 where $z_D = 0.2kpc$) using Toomre's law(1.27). As we see in figures 3.4, 3.5 and 3.6, the dispersion decreases when the radii increases as it happens with the angular velocity, we can therefore say that the motion of bodies is more cahotic when we are closer to the centre. Now we can use (1.32) to calculate the mean angular velocity at each radii. The result is shown in figure 3.7 and we can see that velocity has a maximum in $r \sim 3kpc$ and then decreases.

Now we have a linear grid with $r_i, \Sigma(r_i), V(r_i), \sigma_R(r_i), \sigma_\phi(r_i), \sigma_z(r_i)$ and $\mu(r_i)$.

But this linear grid is not convenient for numerical purposes, so we switch to a new grid where we have a logarithmic scale for radius. The grid now considers the values at each $r_j = \Delta r e^{j\Delta y}$ with $j = 0, ..., N_{log}$, $N_{log} = 300$, $\Delta y = log\frac{R_{min}}{R_{max}}$ Comparing these values of r_j with the radii calculated in the linear grid we can count how many bodies are in each j-cell with equation 3.7.

$$N(r_j) = \frac{N_{disc}}{M_{disc}} \Sigma(r_j) 2\pi r_j \Delta r_j \tag{3.7}$$

Where $N_{disc} = 10^6$ is the total number of bodies. For each j-radius we subsequently calculate $V(r_j)$,

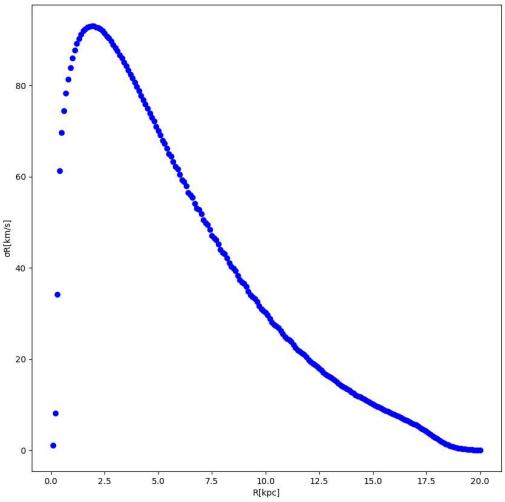

Figure 3.4: Dispersion in radial direction

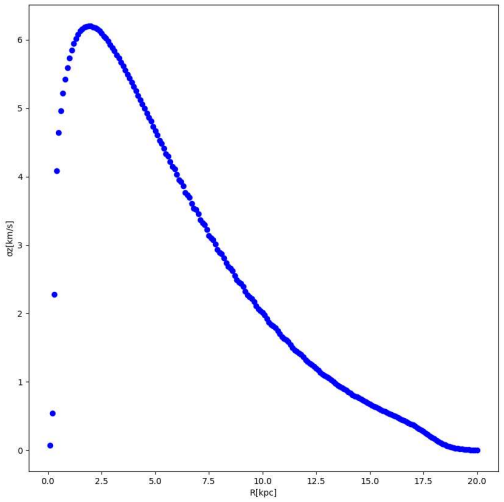

Figure 3.5: Dispersion z direction

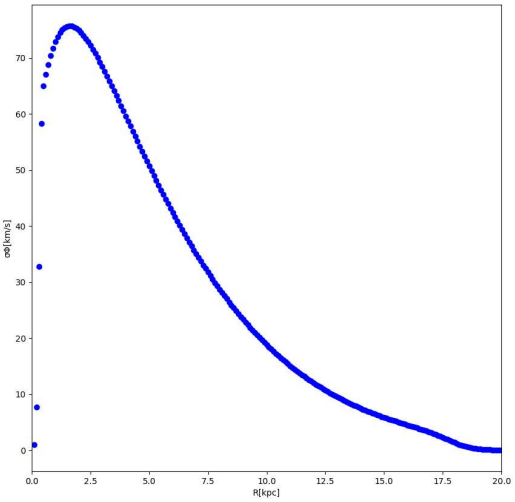

Figure 3.6: Dispersion in angular direction

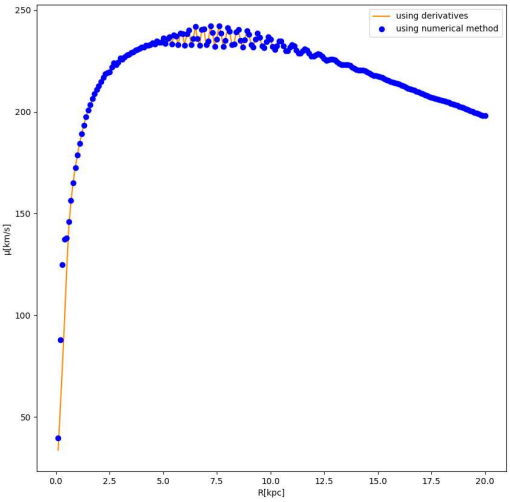

Figure 3.7: Mean angular velocity

$\sigma_R(r_j)$, $\sigma_\phi(r_j)$, $\sigma_z(r_j)$ and $\mu(r_j)$. We consider $i = int(r_j/\Delta r)$ and the $j-$values we look for are calculated by

$$V(r_j) = V(r_i) + \frac{V(r_{i+1}) - V(r_i)}{r_{i+1} - r_i}(r_j - r_i) \tag{3.8}$$

At this point we have the logarithmic grid with all the needed parameters. The $N(r_j)$ objects of each cell are positioned in a uniform distribution around r_j, and their velocities follow a gaussian distribution with standard deviation $\sigma_R(r_j), \sigma_z(r_j), \sigma_\phi(r_j)$. Considering such distributions, we have the cartesian coordinates of space and velocities(1.24).

For the z coordinate we consider (3.4) and produce N_{disc} coordinates.

Finally the N_{disc} coordinates obtained for space and velocity are the initial conditions of the bodies in the disc.

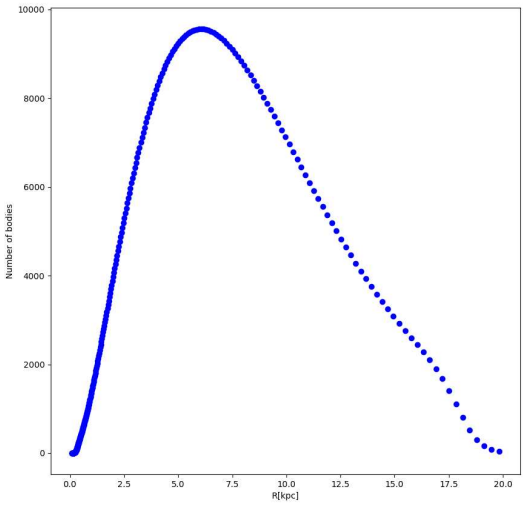

Figure 3.8: Number of bodies depending on the radius

3.1 Test

Once we have the initial conditions, we check if they are compatible with the theory.

3.1.1 Plot of the coordinates

Using the cartesian coordinates we plot the bodies in (3.9). Each colour of this plot represents a different ring of the logarithmic grid. As we see in the figure, the bodies are distributed in a disc with radius of 20kpc.

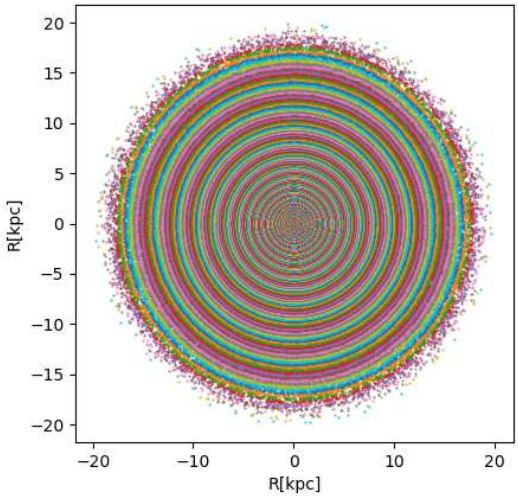

Figure 3.9: Plot of the cartesian coordinates

3.1.2 Density test

Density profile

For this test we consider 100 rings with radii from 0.2 to 20kpc, in each ring we count how many bodies there are after calculating the radii of each one as we did in test 3.1.1. At this point we calculate

the numerical density (3.9) (where ΔN is the number if bodies in the ring with radius between r and $r + \delta r$) for each radius and plot the results figure 3.10.

$$\rho(r) = \frac{\Delta N}{2\pi r \delta r} \tag{3.9}$$

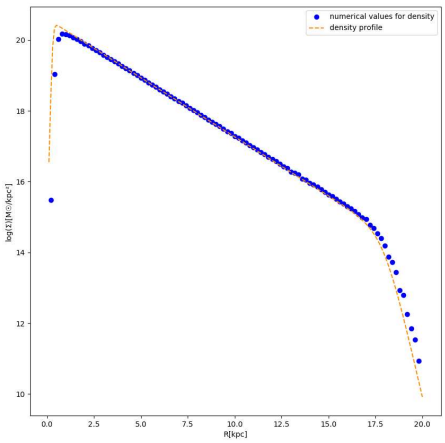

Figure 3.10: Plot for density and radius

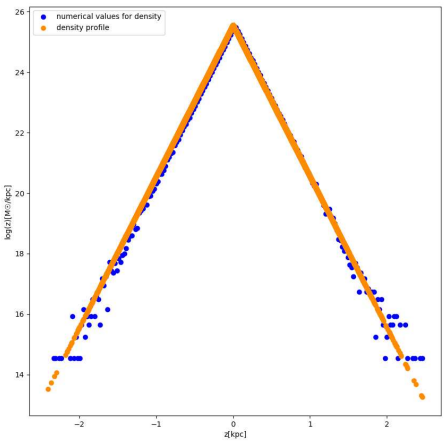

Figure 3.11: Plot for density on z axis

In figure 3.10 it is clear that the results are compatible with what we are expecting. Specifically using a logarithmic scale for density, we can see that there is a linear relation between radii and $log(\rho)$ if are not considered the edges where the correction (3.3) changes the profile. Using the formula of linear interpolation, we obtain a line with slope: -0.308 that, compared to the expected value $-1/R_D = -0.333$, shows that the conditions we obtained are compatible with the model of the galaxy we describe.

Vertical density profile

A similar test can be done for the position of bodies on the z axis. We can consider the maximum value z_{max} of the z coordinates of the initial conditions and divide the disc into 200 intervals between $-z_{max}$ and z_{max}. In each of them we calculate the number of bodies and compare it with (3.4) as we see in figure 3.11. The results are compatible: the slope of the plot with the logarithm of density is 5.00 which is compatible with $1/z_D = 5$.

3.1.3 Mean velocity and dispersion

For each ring considered in 3.1.1 can be calculated the mean velocity of the bodies in the radial, z and angular direction. As we see in figures 3.12 and 3.13 the mean velocity in radial and z directions is close to zero, as we wanted because of the fact that the galaxy we have chosen is in equilibrium. As we get closer to the centre of the galaxy, the mean velocity has a non-zero value because here the bodies are less and are moving really fast, so the situation is more cahotic than it is at bigger radii. Calculating the mean angular velocity and comparing it with the values of the grid, we can see that(in figure 3.14) the two diagrams are superimposable, therefore the results are correct.

In the same way can be calculated the dispersion in radial, z and angular direction and compared with the values of the grid. As we see in 3.15, 3.17, 3.16, we can observe that the dispersions obtained are correct.

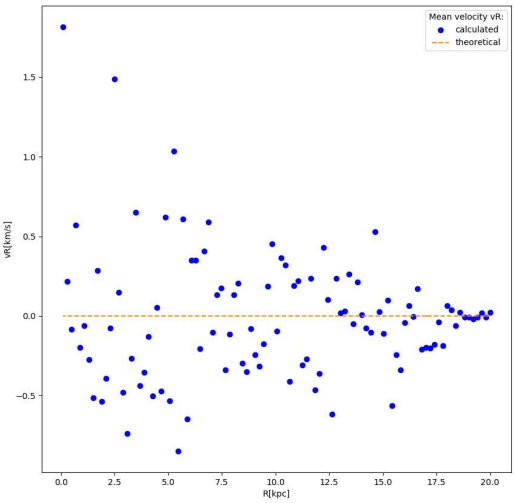

Figure 3.12: Mean radial velocity

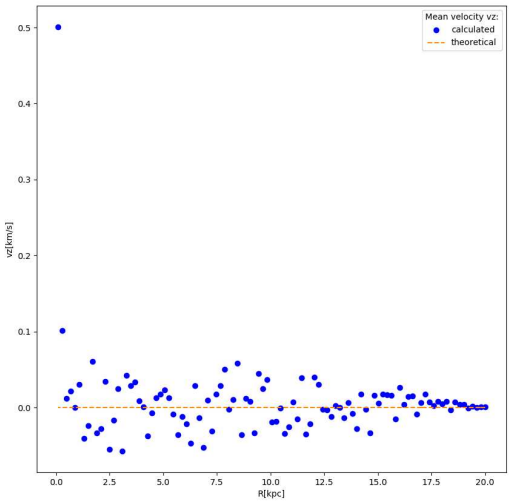

Figure 3.13: Mean z velocity

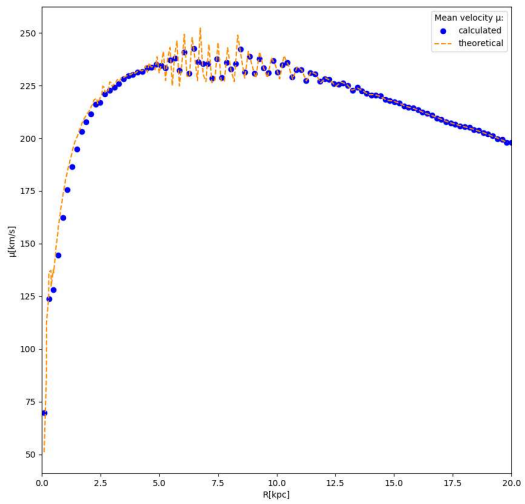

Figure 3.14: Mean angular velocity

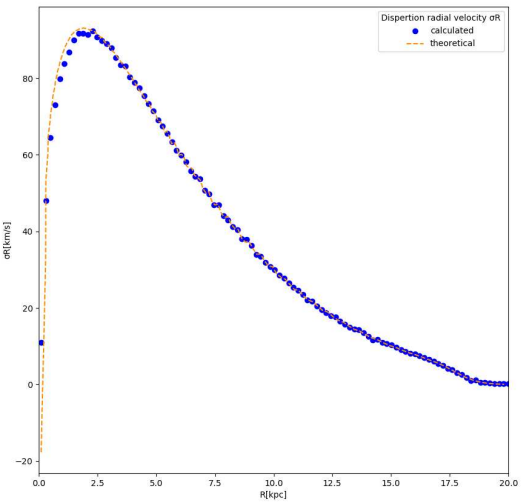

Figure 3.15: dispersion radial velocity

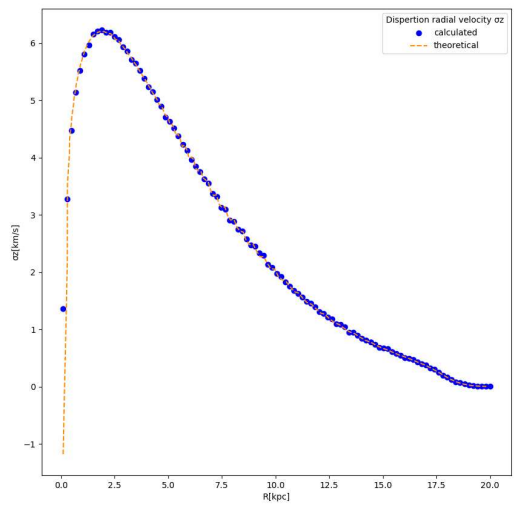

Figure 3.16: Dispersion z velocity

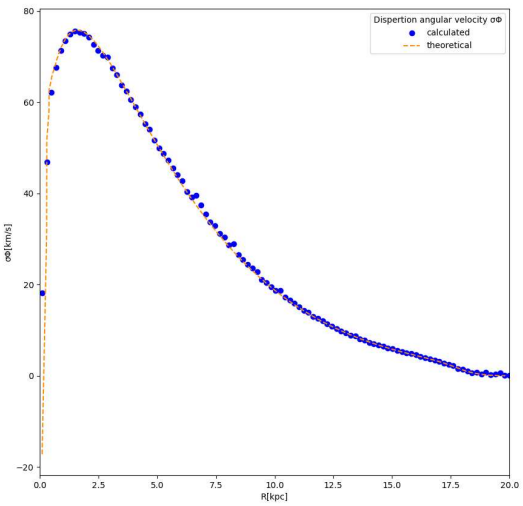

Figure 3.17: Dispersion angular velocity

Chapter 4

Relaxation procedure

4.1 Theory

In order to validate the initial conditions, we used a parallel-mesh code to study the evolution of the system over time and verify if it is stable. This code(described in Kyziropoulos et al. [2016])considers the initial conditions for halo and disc we obtained in the previous sections and puts all the bodies in a box. This box is divided into smaller cubes, for each of them is applied Poissons' equation (1.6) where the density is determined counting how many bodies are in each cell and how much mass is in it. Once we have the density, the potential exerted by one cell on the other can be derived. With this method the acceleration of each body is calculated and then the evolution of the system over time can be described. The spheroidal components of the galaxy can be considered in equilibrium when they are isolated. For the disc the situation is different and we consider the potential of the halo in order to obtain a disc in equilibrium. If the components are together, the situation is not stable and to avoid this condition we consider two stages of relaxation. First of all we relax the halo freezing the disc, then we recompute a new disc with the potential of the halo relaxed. Secondly we freeze the halo and let the disc relax. At this point all the components together are stable and we can check if the system is in equilibrium running a simulation and verifing if the galaxy looks the same over time (in section 5). The reason why we are considering this methond to relax the system and the other possible ways to do it are explained in Barnes and Hernquist [1996], Toomre and Toomre [1972], Hernquist and Quinn [1988], Barnes [1988] , Barnes [1992].

4.2 Halo relaxation

To relax the halo we freeze the disc in a box of 70kpc and let the system evolve until when it looks always the same over time. Once we have relaxed the halo, we consider these new initial conditions and compare them with the previous ones. During the simulation the halo looks always the same, this means that the system is stable even before the relaxation. This is shown in figures 4.1 and 4.2. Using equation (1.21) is calculated the new potential of the halo. The results are shown in 4.3. We also consider the evolution of the halo without the disc in order to verify if it is stable when it is isolated. In the plot we see four different profiles of the potential of the halo:

- The dotted blue line is the Hernquist law for the potential that we imposed at the beginning(2.2).
- The red line is the potential obtained with (1.21) that we already studied and compared with the Hernquist profile in (2.2).
- The green line represents the potential after the relaxation of the halo when it's isolated. We can observe that it's really similar to the analytic profile at bigger radia. At smaller radia the two profiles are slightly different and more bodies are now concentrated in the inner part of the galaxy.

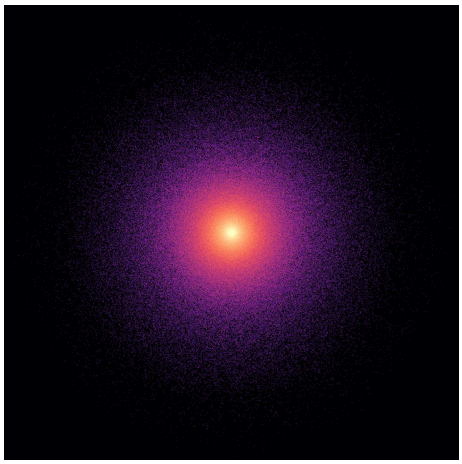

Figure 4.1: Halo after 0.005Gyr

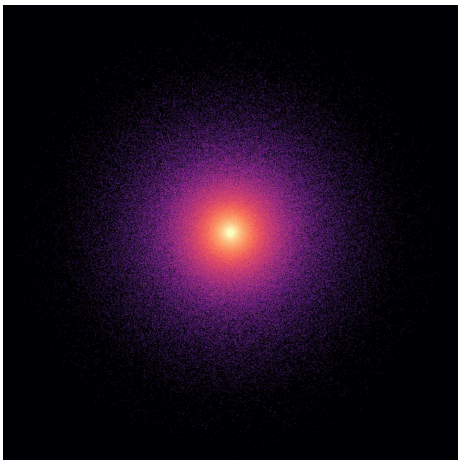

Figure 4.2: Halo relaxed after 1Gyr

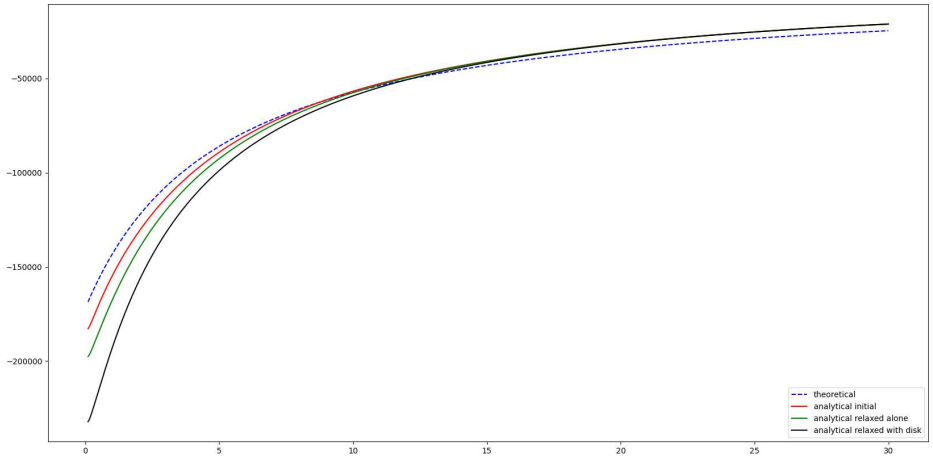

Figure 4.3: Comparison between the potential of the halo before and after relaxation

- The black line represents the potential of the relaxed halo when we freeze the disc. We can see that it is really similar to the analytic profile before relaxation at larger radia. At smaller radia the difference between these profiles can be explained by the fact that after the relaxation more bodies will be in the inner part of the galaxy because they are attracted by the disc bodies, as a consequence the potential in the inner part of the halo will increase.

To study the distribution of bodies of the halo, we can repeat the density test of section 2.3. The results are shown in figure 4.4 where the colours of the plots correspond to the colours of the potential profile we have just explained. We have already described in 2.3 the theoric and analytical profiles before starting the relaxation.

As for the evolution of the halo when it is isolated, we can see that the profile is very similar to the analytical one before the relaxation. This means that the initial conditions of the halo we produced represent a stable model for this component of the galaxy because the distribution of bodies is constant.

If we consider the black line, the situation is slightly different: it is clear that the density is higher at small radia, and lower at bigger radia. The fact that the decrease starts at $r \approx 20kpc$ is not a coincidence: this is the R_{max} of the disc, therefore this is the component involved in the perturbation of the density profile. Maybe this occurs because the disc attracts bodies increasing the density in the inner part of the galaxy. Considering that the total number of bodies is always the same, the rise of density at small radia causes a decrease of this quantity in the outer region of the halo at $r \approx 20kpc$.

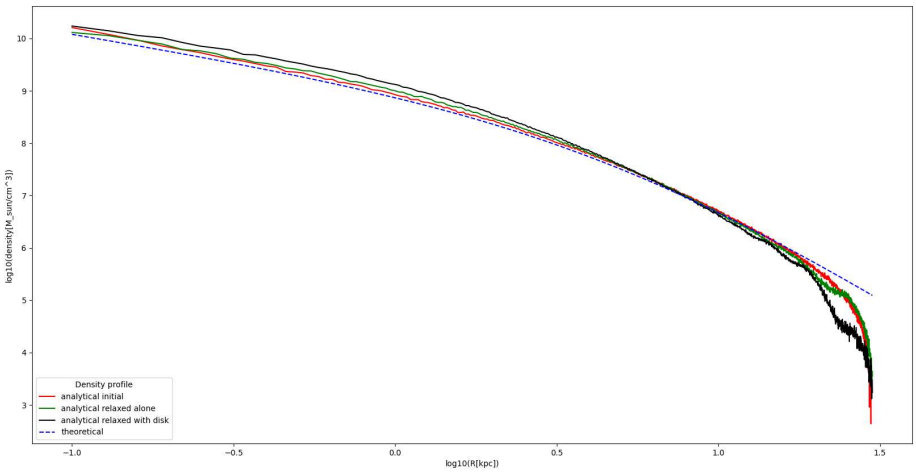

Figure 4.4: Density profiles of the halo after relaxation

Once we have this new relaxed halo we recompute the initial conditions of the disc considering the new halo potential with the same procedure explained in section 3.

The new disc has a density profile similar to the previous one, only at the edges, as we see in figure 4.5, the profile is smoother because after relaxation bodies tend to get this kind of trend. As for the numerical distribution of bodies, this is exactly the same we had for the previous disc. With this new

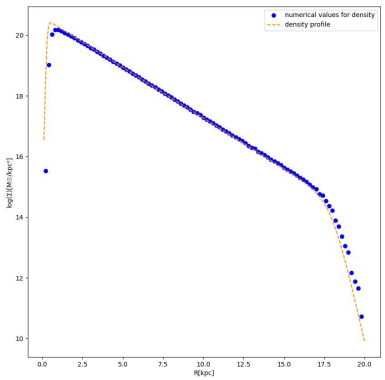

Figure 4.5: Disc density profile before and after relaxing the halo

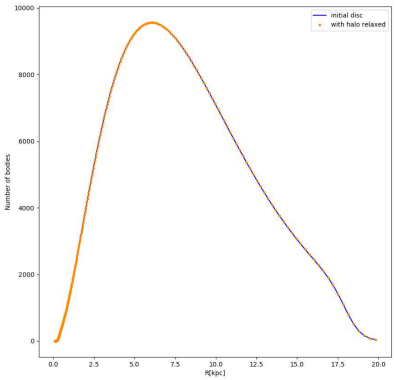

Figure 4.6: Numerical distribution of bodies before and after relaxing the halo

disc we can calculate the new potential shown in figure (4.8) that has a lower value in the inner part and a higher value in the outer region. This is because the distribution is more homogeneous and more bodies have moved towards the centre of the galaxy. This perturbation of the potential causes changes in the value of the angular and epicyclic frequencies that keep the same trend but increase a little their values.

Regarding the velocities, this new disc has mean velocity zero on radial and z direction (as we see in figure 4.9 and 4.10), the dispersion is now smaller if we consider plots 4.11 and 4.13. The velocity on angular direction has a lower value and dispersion as we see in plots 4.14 and 4.12.

The fact that all the bodies are moving less and with less dispersion is compatible with the fact that we are relaxing the system.

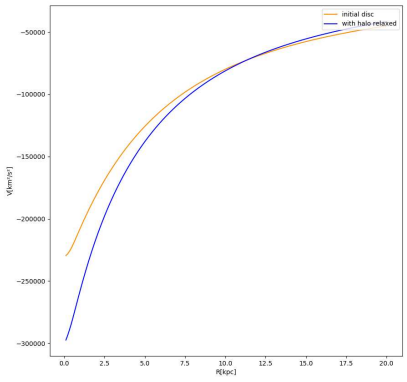

Figure 4.7: Disc potential after relaxing the halo

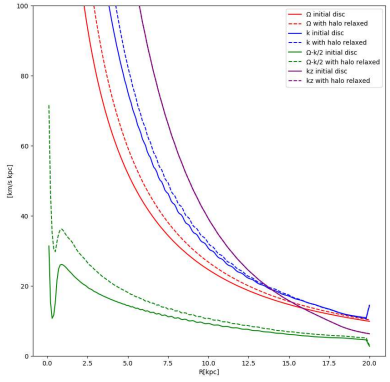

Figure 4.8: Epyciclic and angular frequencies

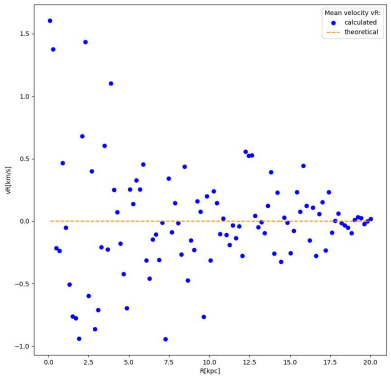

Figure 4.9: Mean velocity on radial direction of disc's bodies after relaxiang the halo

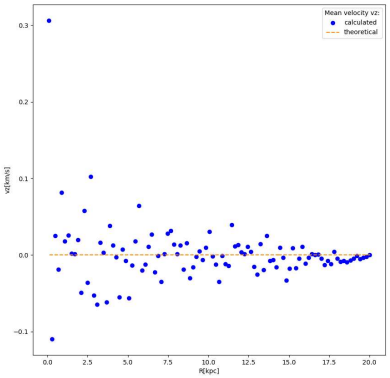

Figure 4.10: Mean velocity on z direction of disc's bodies after relaxiang the halo

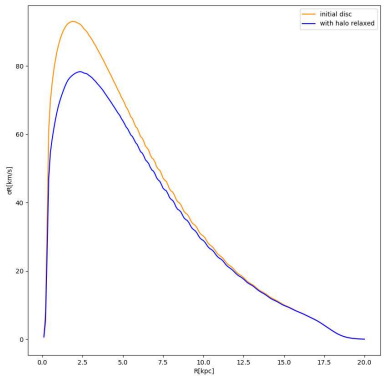

Figure 4.11: Dispersion on radial direction on the disc before and after relaxing the halo

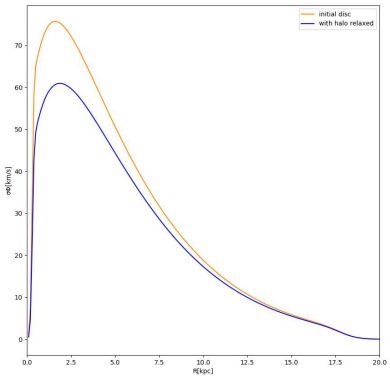

Figure 4.12: Dispersion on angular direction on the disc before and after relaxing the halo

4.3 Disc relaxation

Similarly, we relax the disc freezing the halo. Running the simulation we wait for the disc to keep the same structure over time and compare this new disc with the previous one. Figure 4.15 shows the xy projection of the disc after 0.005Gyg with the frozen halo. The galaxy does not look completely uniform, probably because at the centre of the galaxy the bodies are moving chaotically and this

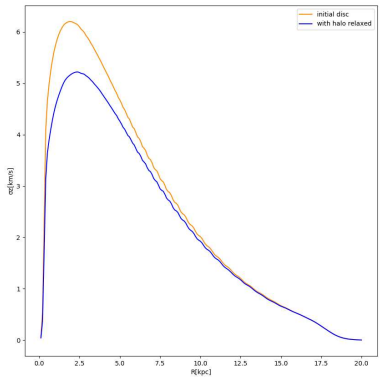

Figure 4.13: Dispersion on z axis direction on the disc before and after relaxing the halo

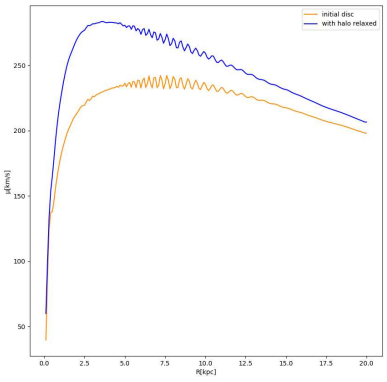

Figure 4.14: Mean angular velocity on angular direction before and after relaxing the halo

causes a phenomenon similar to density waves where regions of high density are followed by regions of lower densities as we see in the plot. This occurs also in the yz plot in 4.17, where in the inner part of the galaxy the thickness does not look like the profile 3.4. After 1Gyr the disc looks like in figures 4.16, 4.18 and the waves disappear. The disc has a uniform and constant distribution of bodies, therefore we reached a stable condition for this component. It is clear from 4.16 that some spirals have formed, these non axisymmetric features are caused by swings in the potential(this phenomena is explained in Toomre [1981]). In 4.19 is shown the new density profile which is very close to the density profile of

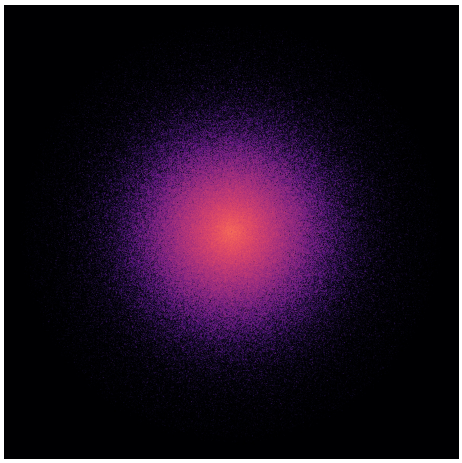

Figure 4.15: Disc after 0.005Gyr(xy plot)

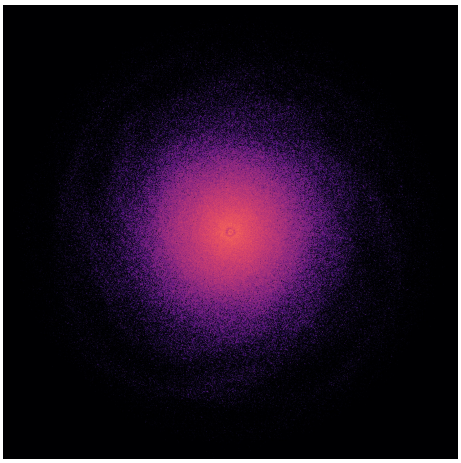

Figure 4.16: Disc relaxed after 1Gyr(xy plot)

the disc after relaxing the halo, the only difference is at $r \approx 15kpc$ where there is a small perturbation of the density. In 4.20 is plotted the new potential of the disc with the orange line. The potential is a little different in the inner part probably because in this region of the galaxy bodies are moving really fast and the model is not a perfect approximation. With this new potential, calculated using equation (3.6), the new epicyclic and angular frequencies shown in figure 4.21 can be measured.

We can compute the velocities in each direction with the correspondant dispersion using the method explained in section 1.3, the results are plotted in figures 4.22, 4.23, 4.24 and 4.25. The profiles are very similar, so that, once we have relaxed the halo, the initial conditions of the disc we produced are compatible with a stable system. Finally, we have equilibrium conditions both for the halo and the disc.

We did not take into account the bulge in this process of relaxation to simplify the situation. However considering that the halo was in equilibrium, the bulge should be stable too because its initial conditions are produced in the same way of the halo.

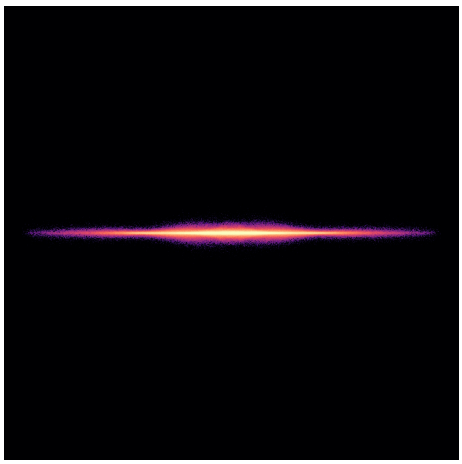

Figure 4.17: Disc after 0.005Gyr(yz plot)

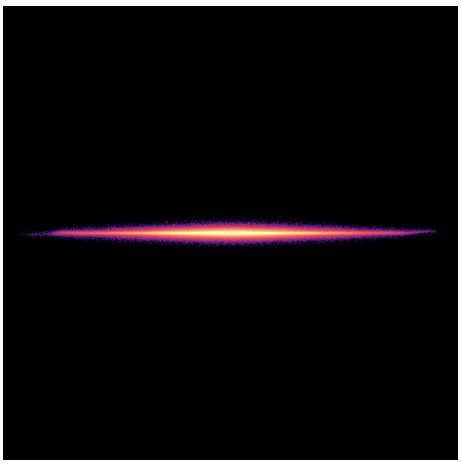

Figure 4.18: Disc relaxed after 1Gyr(yz plot)

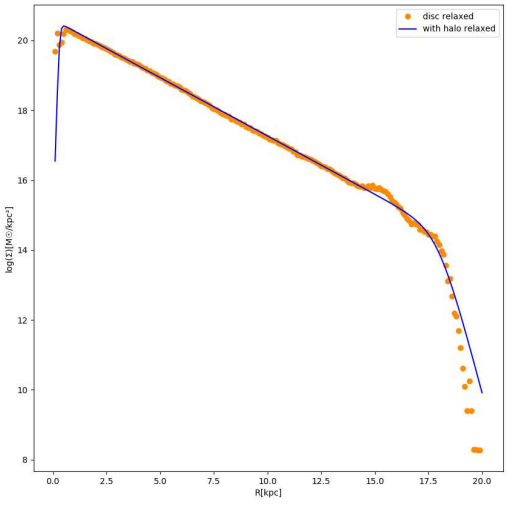

Figure 4.19: Density profile of the disc before and after relaxation

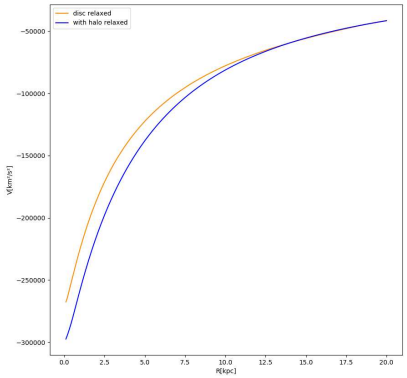

Figure 4.20: Disc potential after relaxing the disc

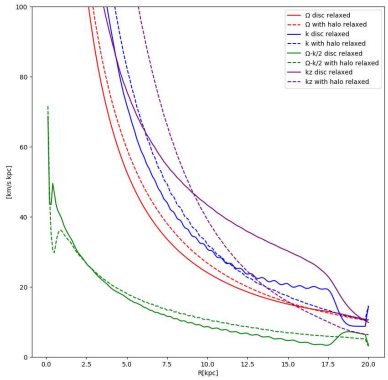

Figure 4.21: Epyciclic and angular frequencies

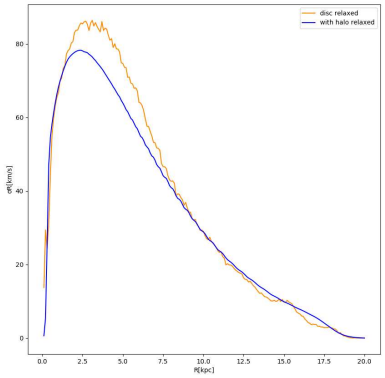

Figure 4.22: Dispersion on radial direction on the disc before and after relaxing the halo

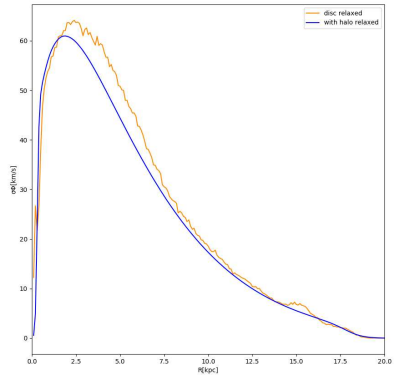

Figure 4.23: Dispersion on angular direction on the disc before and after relaxing the halo

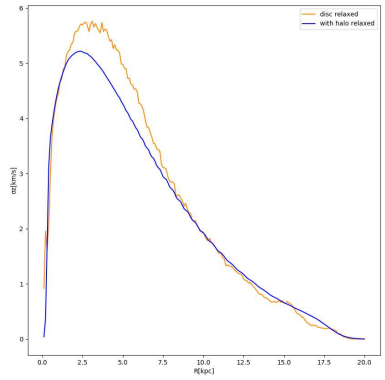

Figure 4.24: Dispersion on z axis direction on the disc before and after relaxing the halo

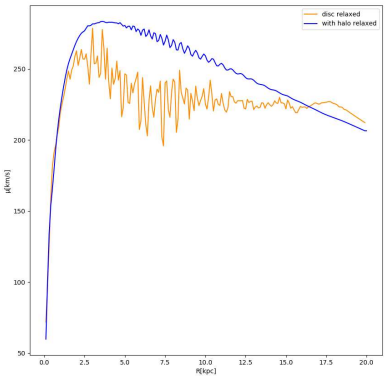

Figure 4.25: Mean angular velocity on angular direction before and after relaxing the halo

Chapter 5

Final equilirum

Once both the halo and the disc have been relaxed we can put them together and run a new simulation(see similar simulations in art [1975], Sellwood and Carlberg [1984], Sellwood and Carlberg [2014]). If the system keeps always the same structure, we can finally say that the initial conditions we have produced are in equilibrium. In the following images is shown the galaxy edge-on and face-on after relaxing it for 0.005Gyr, 0.25Gyr, 0.5Gyr, 0.75Gyr, 1Gyr. The plots are really similar, therefore we can think that the galaxy is stable. In order to verify this statement, we analyze the distribution of bodies and velocities during the simulation repeating the tests we did in the previous sections.

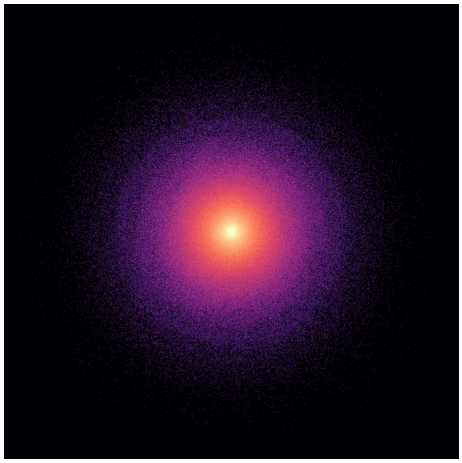

Figure 5.1: Disc and halo at 0.005Gyr

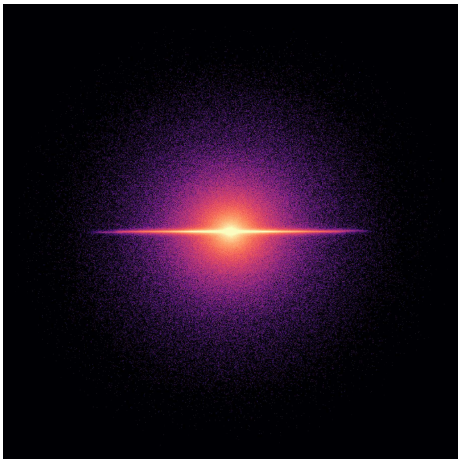

Figure 5.2: Disc and halo at 0.005Gyr

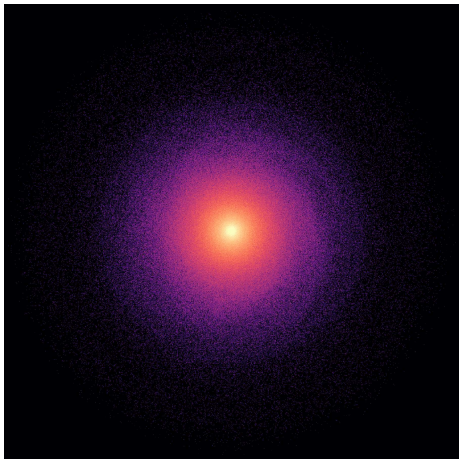

Figure 5.3: Disc and halo after 0.25Gyr

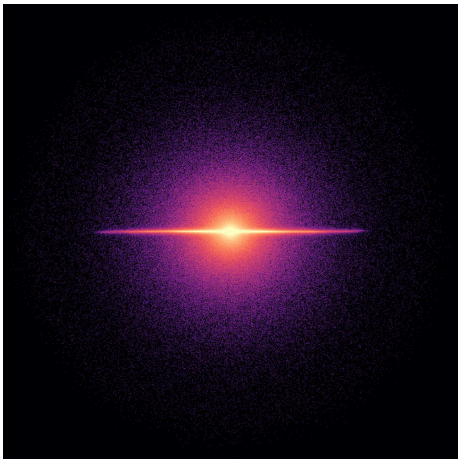

Figure 5.4: Disc and halo after 0.25Gyr

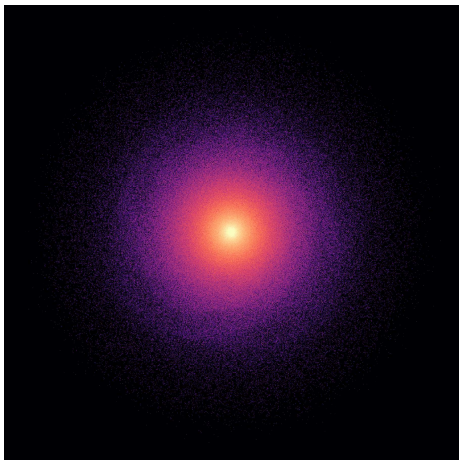

Figure 5.5: Disc and halo after 0.50Gyr

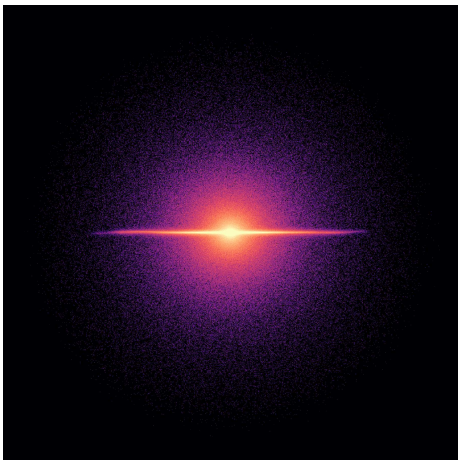

Figure 5.6: Disc and halo after 0.50Gyr

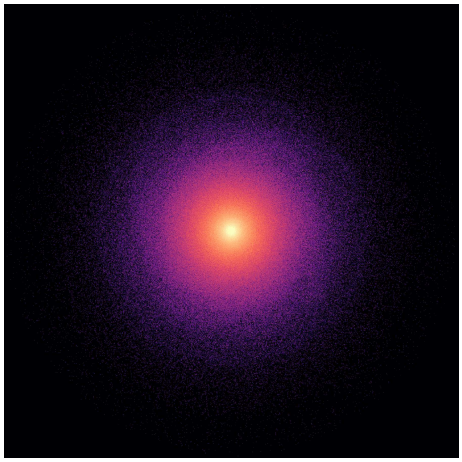

Figure 5.7: Disc and halo after 0.75Gyr

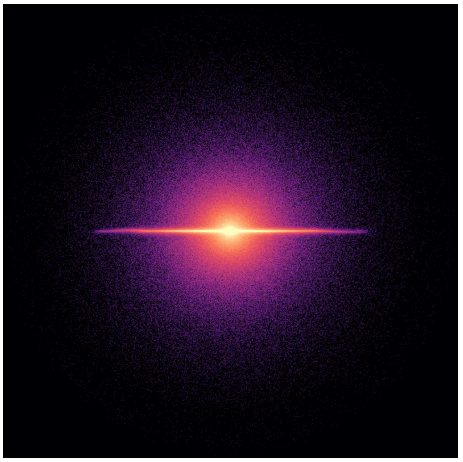

Figure 5.8: Disc and halo after 0.75Gyr

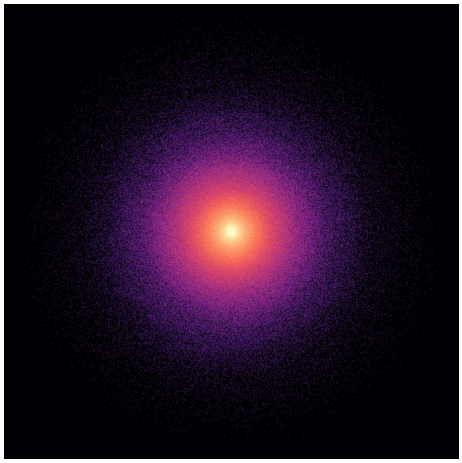

Figure 5.9: Disc and halo after 1Gyr

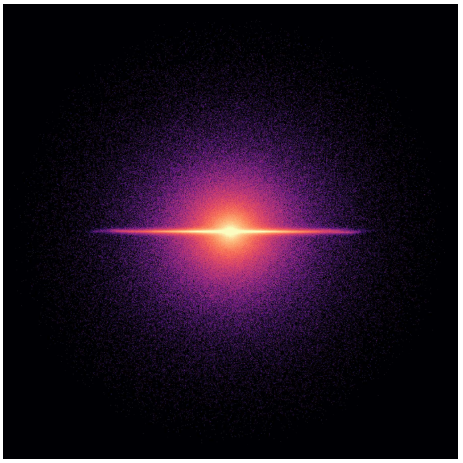

Figure 5.10: Disc and halo after 1Gyr

We define the density profile using the procedure described in section 2.3 both for the halo and the disc at different times. Analyzing the plots 5.11 and 5.12, we can see that the profile is the same over time, therefore the system can be considered in equilibrium. There are only small perturbations for the halo at $r \approx 20kpc$, this is the radius where the disc ends. Probably this is the reason why there is not complete equilibrium at this r. As for the disc, the perturbations of the density profile occur at radius $\approx 17kpc$. In the previous sections we saw this event taking place before the cut off radius where there is some instability. For the disc we can also consider the evolution of mean velocity on angular direction and dispersion of velocities. The plots in figure 5.13, 5.14, 5.15 and 5.16 show that

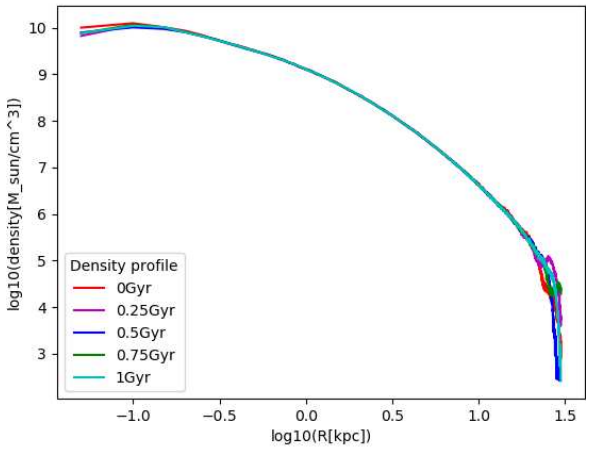

Figure 5.11: Halo density profiles

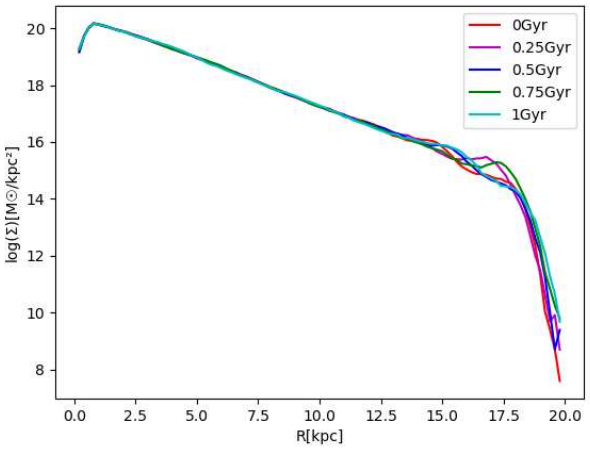

Figure 5.12: Disc density profiles

velocities and dispersions keep the same trend over time.

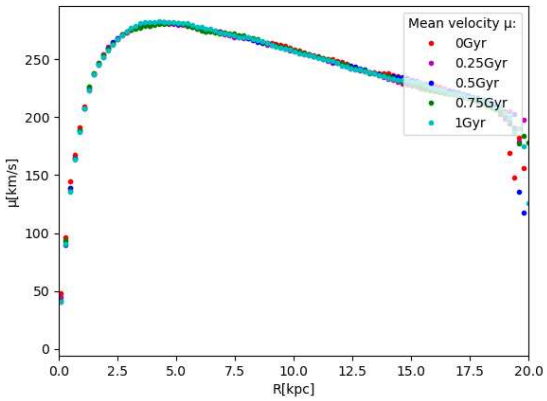

Figure 5.13: Mean angular velocity profiles

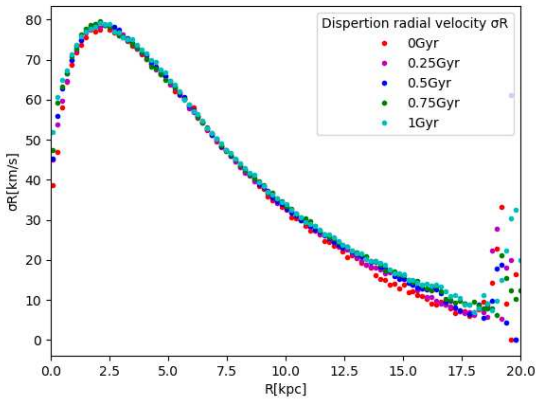

Figure 5.14: Dispersion of radial velocity

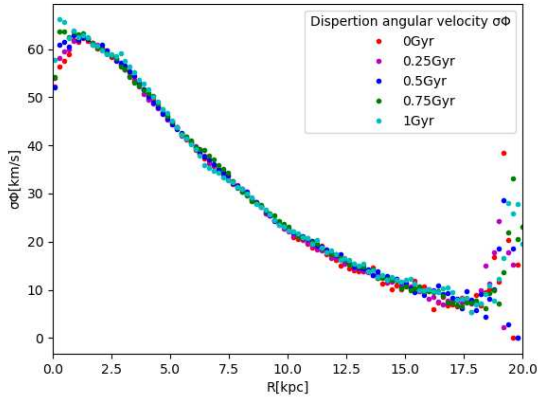

Figure 5.15: Dispersion of angular velocity

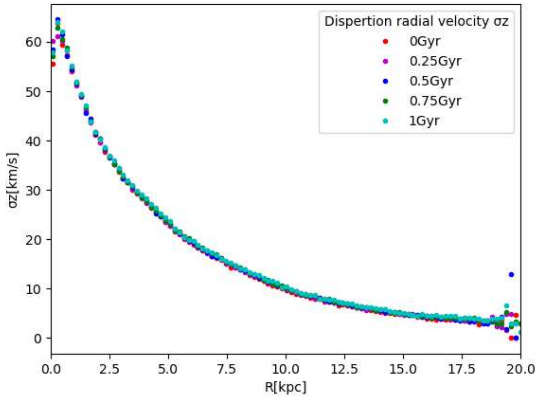

Figure 5.16: Dispersion of velocity on z axis

In conclusion we can say that the galaxy in this section is stable because it keeps the same features over time, therefore the procedure we used to determine these initial conditions leads to a galaxy in equilibrium.

Bibliography

Dynamics of stellar systems: proceedings from IAU Symposium no. 69 held in Besancon, France, September 9-13, 1974., volume 69, January 1975.

Joshua E. Barnes. Encounters of Disk/Halo Galaxies. , 331:699, August 1988. doi: 10.1086/166593.

Joshua E. Barnes. Transformations of Galaxies. I. Mergers of Equal-Mass Stellar Disks. , 393:484, July 1992. doi: 10.1086/171522.

Joshua E. Barnes and Lars Hernquist. Transformations of Galaxies. II. Gasdynamics in Merging Disk Galaxies. , 471:115, November 1996. doi: 10.1086/177957.

James Binney and Scott Tremaine. *Galactic dynamics*. 1987.

Lars Hernquist. An Analytical Model for Spherical Galaxies and Bulges. , 356:359, June 1990. doi: 10.1086/168845.

Lars Hernquist and P. J. Quinn. Formation of Shell Galaxies. I. Spherical Potentials. , 331:682, August 1988. doi: 10.1086/166592.

P. E. Kyziropoulos, C. Efthymiopoulos, G. A. Gravvanis, and P. A. Patsis. Structures induced by companions in galactic discs. , 463(2):2210–2228, December 2016. doi: 10.1093/mnras/stw2084.

J. A. Sellwood and R. G. Carlberg. Spiral instabilities provoked by accretion and star formation. , 282:61–74, July 1984. doi: 10.1086/162176.

J. A. Sellwood and R. G. Carlberg. Transient Spirals as Superposed Instabilities. , 785(2):137, April 2014. doi: 10.1088/0004-637X/785/2/137.

A. Toomre. What amplifies the spirals. In S. M. Fall and D. Lynden-Bell, editors, *Structure and Evolution of Normal Galaxies*, pages 111–136, January 1981.

Alar Toomre and Juri Toomre. Galactic Bridges and Tails. , 178:623–666, December 1972. doi: 10.1086/151823.